Journal of Low Temperature Physics
https://doi.org/10.1007/s10909-021-02636-1

Recent Experimental Studies on Solid ^{4}He

Moses H. W. Chan[1]

Received: 31 July 2021 / Accepted: 11 October 2021

Abstract
In this article, we review the experimental studies in pursuit of supersolidity and on recent studies of mass flow through solid ^{4}He samples.

Keywords Solid helium · Supersolidity · Luttinger liquid

1 Introduction

John Reppy is renowned for his seminal role in elucidating the nature of superfluidity in liquid helium. His most notable contributions include the elegant gyroscopic experiments in clarifying the properties of persistent currents [1], experiments with Bishop in confirming the Kosterlitz-Thouless vortex-anti-vortex unbinding theory of two-dimensional superfluidity in helium films [2] and the studies of helium film adsorbed in different porous media that clarified the effect of disorders and impurities in a system undergoing continuous phase transition [3].

The tool of choice of his helium film experiments, which he perfected to great precision and utilities is the high mechanical Q torsional oscillator (TO). TO measures the superfluid fraction of helium films adsorbed on planar and porous media surfaces. The decoupling of the superfluid fraction from the substrate inside a torsion bob leads to a drop of the resonant period when the TO is cooled into the superfluid state. The resonant period of the TO, τ, is given by $2\pi\ (I/\ \kappa)^{1/2}$, where I and κ are, respectively, the rotational inertia of the torsion bob and the spring constant of the torsion rod. The introduction of liquid helium in the normal state into the torsion bob, typically through a hollow torsion rod increases I and hence the resonant period ($\Delta\tau_o$). This increase is also known as the mass loading of the helium film. The decoupling of the superfluid below the transition temperature will lead to a drop in the resonant ($\Delta\ \tau_s$). The ratio ($\Delta\tau_s/\Delta\tau_o$) is the superfluid fraction or the nonclassical rotational inertia fraction (NCRIF). For helium films adsorbed on or confined

✉ Moses H. W. Chan
mhc2@psu.edu

[1] Department of Physics, The Pennsylvania State University, University Park, PA 16802, USA

Published online: 10 November 2021

in a tortuous porous substrate, a correction will be needed to get the correct superfluid fraction. If the TO is carefully constructed and the torsion rod is made from high mechanical Q material, the resonant period can be stabilized and resolved to a fraction of a nanosecond (ns) out of a resonant period of ~ 1 or 2 milli-second (ms). For a ^{4}He film adsorbed on a high surface area substrate, TO can easily resolve the superfluid decoupling of 1% of a monolayer.

The TO also played a very important role in the search of supersolidity or superfluidity in solid ^{4}He. The possibility of superfluidity in solid ^{4}He was considered by Andreev and Liftshitz [4], Chester [5, 6], Reatto [7], Leggett [8] and others in the 1960 and 1970s. These papers suggested that the existence of a supersolid state cannot be ruled out on theoretical grounds. These papers spawn many experimental searches for superfluidity in solid ^{4}He in the 1970s and 1980s [9–13], including a TO study by Bishop, Paalanen and Reppy [13]. However, none of these searches found evidence of supersolidity. Bishop, Paalanen and Reppy concluded that superfluid fraction or nonclassical rotational inertia (NCRI) in solid ^{4}He, if exists, is less than $5 \times 10^{-6.}$

2 Apparent Signatures of Supersolidity

John Goodkind and his collaborators carried out a series of ultrasound experiments in the 1990s searching for signatures of Bose–Einstein condensation in solid ^{4}He [14]. In a 2002 paper [15] Goodkind reported evidence of Bose-condensation of thermally activated vacancies at temperatures above 200 mK. While the reported results are not expected for a supersolid state, these unusual results prompted Eunseong Kim and Moses Chan (KC) of Penn State to initiate new TO experiments to search for superfluidity in solid ^{4}He confined in porous gold [16]. The motivation to look for superfluidity in solid ^{4}He inside a random porous structure is that such samples are expected to be heavily populated with defects and vacancies and the Bose-condensation of these vacancies could induce the sample into the supersolid phase. A drop in the resonant period of 15 ns was found below 200 mK. The OD and ID of the hollow Be-Cu torsion rod of this TO are, respectively, 1.0 and 0.4 mm. KC was concerned that the observed period-drop may be a result of the stiffening of solid ^{4}He inside the torsion rod at low temperature [17]. To check this possibility, they built a new TO with a torsion rod with OD and ID of 2.2 and 0.4 mm with a disk of porous Vycor glass secured inside the torsion cell. By increasing the OD of the torsion rod from 1.0 to 2.2 mm, the contribution of solid ^{4}He inside the torsion rod to the spring constant of the torsion rod and the stiffening effect at low temperature will be $(2.2)^4$ or 24 times smaller. Since the resonant period of the Vycor glass TO is ~ 3 times smaller than the porous gold TO, if the observed period-drop found with the porous gold TO is indeed a torsion rod effect then the same effect should be 70 times smaller. What KC found with the Vycor glass TO is that the resonant period shows a drop that begins at 175 mK that saturates to 17 ns at 30 mK. Since the size of the period-drop is nearly equal to that found in the porous gold TO, it cannot be a torsion rod effect. In addition, the size of the period-drop is found to decrease systematically with the maximum oscillating speed of the torsion bob. This reduction is consistent with the critical velocity behavior in superfluid ^{4}He films. These

findings led KC to publish the results under the title, 'Probable observation of a supersolid phase' [18]. An unexplained finding at the time is the increase in the onset temperature with increasing concentration of ^{3}He impurities in the solid samples.

The 'positive' results from solid ^{4}He in porous Vycor glass prompted KC to carry out a new TO study on bulk solid ^{4}He. The bulk solid ^{4}He samples were confined in an annulus with a width of 1 mm and an OD of 1 cm. Four different solid samples at pressure ranging from 26 to 65 bar were studied. All four samples show period-drops below 200 mK. However, the apparent superfluid or nonclassical rotational inertia fraction (NCRIF) of the samples varies from 7×10^{-3} to 1.7×10^{-2} without systematic dependence on sample pressure. For comparison, the apparent NCRIF found in solid ^{4}He in porous Vycor glass and porous gold [19], with tortuosity corrections, is 2.5×10^{-2} and 1.2×10^{-2}, respectively. Consistent with the findings in the Vycor TO, the period-drops in the bulk solid samples also show an apparent critical velocity near 10 μm/s. A control experiment with a TO with a metal insert wedged into annulus sample space was also carried out. This insert was added to block any possible oscillatory superfluid flow. The measured period-drop of this blocked annulus TO was found to be about a factor of 70 smaller than expected if there is no block. The small period-drop found in the blocked annulus cell was attributed to an irrotational flow effect of a superfluid in a blocked channel of finite width. The result of this control experiment bolstered the superflow interpretation and emboldened KC to publish these results with the title 'Observation of Superflow in Solid helium' [20]. As we shall show below there is an alternative, non-superflow interpretation that explains this reduction in the period-drop.

The news of supersolidity raised a great deal of interest in the low-temperature physics community and brought John Reppy out of his retirement [21] to join the effort. The first confirmation of Penn State's results did come from his laboratory [22]. Within a few years, there were many other reports confirming the results from Penn State [23–29]. While the observed period-drops in all the TO experiments show similar temperature dependence, the magnitude of the apparent NCRIF varies from experiment to experiment. For solid ^{4}He confined in porous media, the reported apparent NCRIF varies from 3×10^{-4} to 7×10^{-2} [18, 19, 26, 30]. For bulk solid samples, the apparent NCRIF ranges from 3×10^{-5} to 0.18 [22–29]. A few experiments were carried out to correlate the magnitude of the apparent NCRIF with the quality of the ^{4}He crystals. In the end, no correlation was established. The ^{3}He impurity effect found in the Vycor experiment was replicated in bulk solid samples [31]. It was found that the onset temperature of the period-drop shows a monotonic increase with ^{3}He concentration. For a ^{4}He sample with 30 parts per million of ^{3}He, the onset temperature of the period-drop is found to be at 1.25 K, for a sample with 1 part per billion of ^{3}He, the onset temperature is found to be close to 80 mK. A summary of these and other experiments published before 2013 can be found in a review article in the Journal of Low-Temperature Physics [32].

3 An Alternative Interpretation

The breakthrough in revealing an alternative interpretation of the period-drops in TOs came from a 2007 shear modulus experiment. Day and Beamish [33] found an 11% increase in the shear modulus of solid ^{4}He when the solid sample was cooled through 100 mK. The increase in the shear modulus, as shown in Fig. 1, shows temperature and ^{3}He concentration dependences that track quantitatively the period-drops results in TO experiments. The increase in shear modulus is due to the binding of ^{3}He atoms on the dislocations in solid ^{4}He with a binding energy of $E_D/k_B = 0.7$ K. With decreasing temperature progressively more ^{3}He atoms bind onto the dislocation lines, thus shortens the pinning lengths of the dislocation network and stiffens the sample. The tracking of the two phenomena suggests that the period-drops in TOs could be the consequence of the stiffening of the solid sample. As noted above, the stiffening of the solid ^{4}He inside the hollow torsion rod increases the spring constant of the torsion rod which can lead to a drop in the resonant period [17]. Beamish and collaborators carried out an analysis and showed the period-drops reported in many TO experiments can be explained away by this torsion rod effect [34]. This is not the case for many other TO experiments where the observed period-drops cannot be the torsion rod effect because OD and ID of the torsion rods in these TOs are, respectively, sufficiently large and small. There are, however, other mechanisms through which shear modulus stiffening of solid ^{4}He can affect the resonant period. Since the solid ^{4}He sample is a part of the torsion bob, an increase in the shear modulus of solid ^{4}He sample stiffens and increases the mechanical Q of the torsion bob and reduces the period. Maris [35] calculated such an effect for an isotropic solid ^{4}He sample inside an infinitely rigid torsion cell. For a cylindrical solid sample of 1 cm in height and diameter oscillating at 1 kHz, a 20% increase in the shear modulus of helium results in an apparent NCRI of 1×10^{-4}. This apparent NCRI scales with the magnitude of the shear modulus increase and with the physical dimension of the solid ^{4}He sample. A 10 to 20% increase in shear modulus is

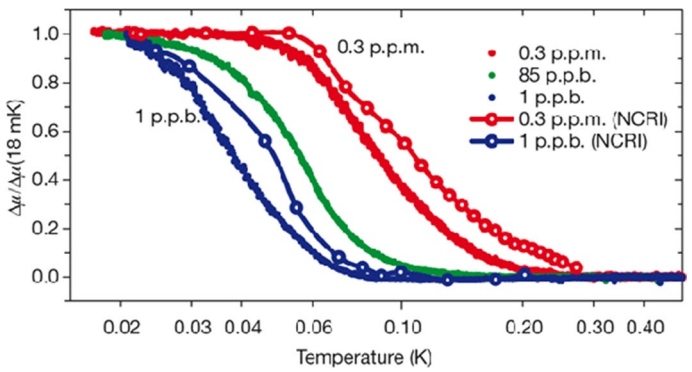

Fig. 1 Shear modulus (solid dots) and normalized torsional oscillator period-drop or apparent NCRI results (open circles from [20, 31]) for solid samples of three different ^{3}He concentrations (adapted from [33]) (Color figure online)

typically found when a polycrystalline sold ^{4}He sample is cooled from 200 to 20 mK. Remarkably, in single crystal samples a total change of 80% has been observed [36]. For TOs with a more complicated geometry and a torsion cell that is not infinitely rigid, this shear modulus effect on the resonant period can be calculated more easily numerically by finite element method [37, 38]. If a TO is not perfectly rigid different components of the torsion cell will not oscillate in phase and the solid ^{4}He sample will act as a 'glue' in improving the mechanical coupling of these different components. In such a situation the stiffening of the shear modulus of solid ^{4}He increases the efficacy of this mechanical coupling and enhances the Q of TO which will lead to a drop in the resonant period. When an insert was wedged into the annulus of the control experiment on bulk solid ^{4}He [20], the rigidity and Q of the TO were improved. With such an enhancement in Q, the additional stiffening of the TO due to the increase in the shear modulus of solid ^{4}He becomes, apparently, 70 times less important.

There is yet another mechanism that magnifies the effect of shear modulus increase of solid ^{4}He. If the torsion rod is anchored on a very thin metal plate of the torsion cell, solid ^{4}He adhered to this plate may play a non-negligible supplementary role to the metal plate in transmitting the torque from the torsion rod to the body of the TO in maintaining the oscillatory motion. In this situation, an increase in the shear modulus of solid ^{4}He also increases the Q of the TO and leads to a drop in the resonant period. This mechanism is particularly relevant to Ref. [18].

Reppy carried out an experiment that supports the interpretation of the observed period-drop to be a consequence of shear modulus stiffening rather than NCRI. He plastically deformed the solid ^{4}He sample in situ, the resonant period of the TO shows a change at high rather than at low temperature. This is not consistent with the notion of a superfluid [39].

4 The Upper Limit of Nonclassical Rotational Inertia Fraction in Solid ^{4}He

Chan's group took a direct approach by employing rigid TOs that reduce shear modulus stiffening effect of solid ^{4}He samples. They built TOs with a solid metal body and used solder instead of epoxy to seal the sample space. Solid ^{4}He samples are confined as annular sheets on the outer rim of the torsion body to maximize any possible superfluid response. In order to minimize the shear modulus effect, the width of the annular sample space is kept narrow [35]. The ^{4}He samples were introduced into the torsion cells via a thin (0.3 mm OD, 0.1 mm ID) and soft nickel capillary instead through a hollow torsion rod. Measurements with such a TO (resonant period ~ 2.56 ms) found 'period-drops' at low temperature of ~ 0.06 ns, consistent with that expected for a 20% enhancement in shear modulus and on the order of the resolution of the measurements. Since mass loading of the solid sample is ~ 14,400 ns, this means, if superfluidity does exist in bulk solid ^{4}He, the nonclassical rotational inertia is less than 4×10^{-6} [40]. This upper limit is nearly the same as that set by Ref. [13].

The experiments with rigid TOs made a strong case that the observed period-drops in bulk solid ^{4}He are due to shear modulus stiffening rather than superfluidity. Such a conclusion cannot be extended directly to the results of solid ^{4}He in Vycor. The typical length between neighboring nodes in a dislocation line network is more than 10 μm, orders of magnitude longer than the dimension of the pores in Vycor at 7 nm. This means there is no dislocation network for solid ^{4}He in Vycor and hence no shear modulus enhancement due to the binding of ^{3}He impurities. This raises the question on what is responsible for the 17 ns period-drop observed in the 2004 Vycor experiment [18]. In the 2004 Vycor experiment, the Vycor disk was sealed inside the torsion cell. Since ^{4}He must be allowed to infuse from the hollow torsion rod into the Vycor disk, a thin gap is left between the top plate of the torsion cell and the Vycor disk. When the Vycor disk is pressurized with solid ^{4}He, the gap is filled with bulk solid ^{4}He. The thickness of the Be-Cu top plate, anchoring the torsion rod, was kept thin to 0.5 mm to reduce the mass of the TO. As noted above, in such a geometry, an increase in the shear modulus of the thin solid ^{4}He layer increases the Q of the TO and causes a drop in the resonant period. A finite element simulation shows that if the thickness of the solid ^{4}He layer is 50 μm, a reasonable estimate of the width of the gap in the torsion cell, then the shear modulus stiffening can account for the observed 17 ns period-drop [41]. To confirm this scenario, Dukyoung Kim built a 'naked' Vycor TO without any metal shell that can hold bulk solid ^{4}He around the Vycor disk (Fig. 2). The open porous channels in Vycor were sealed instead with a thin layer of epoxy painted directly on the outer surface of the disk and helium is brought via a capillary inserted into the center of the disk. Since the pores in Vycor has dimension of only 7 nm, the epoxy layer can easily hold the pressure of the solid ^{4}He sample inside the porous structure. In contrast to the 2004 experiment, no sign of any period-drop was detected with this new 'naked' or bulk solid ^{4}He free TO (Fig. 2). The resolution of the resonant period at 0.1 ns translates

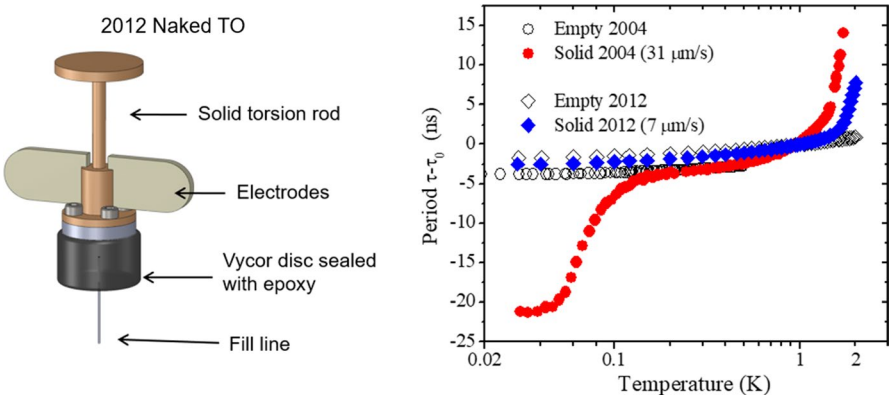

Fig. 2 (Left) A drawing of the 2012 'naked' Vycor TO. (Right) Resonant period versus temperature of solid ^{4}He in the 2004 ([18]) and the 2012 ([41]) Vycor TOs. Empty cell curves are also shown. The period-drop found in the 2004 experiment is due to shear modulus stiffening of a thin bulk solid ^{4}He layer inside the TO. The curves are shifted for easy comparison by adjusting τ_0. Figure adapted from [41]. (Color figure online)

to an upper limit of NCRI of solid ^{4}He in Vycor of no more than 2×10^{-5} [41]. This result also confirmed that the 17 ns period-drop found in the 2004 experiment is due to shear modulus stiffening of the thin bulk solid ^{4}He layer inside the torsion cell. In another experiment, Mi and Reppy built a Vycor TO with two resonant modes with different resonant frequencies. The period shift response shows a strong dependence on the resonant frequency, unlike the behavior expected for a superfluid [42].

Experiments of pressure-driven flow in solid ^{4}He also cast doubts on the existence of NCRI in solid ^{4}He [43–45]. These experiments placed upper limit on the flow velocity to be many orders of magnitude below the 'critical velocities' suggested by the 2004 experiments [18, 20]. Thermodynamic experiments along the melting curve [46, 47] did not find any evidence of a transition to a supersolid state. Heat capacity measurements [48–50] found a peak after the regular T^3 subtraction. For a solid sample in coexistence with superfluid, the peak is found near 60 mK with a height of 5 μJmol^{-1} K^{-1}. For a solid sample of the coexistence curve, the peak is ten times larger and located near 100 mK. It is not clear what the physical origin of this peak is. Other experiments including dielectric constant [51, 52] and fourth sound [53, 54] measurements also did not find any evidence of supersolidity. A neutron scattering experiment reported the observation of superfluid components in the quasi-2D double liquid layer at the interface of solid ^{4}He and aerogel [55]. Other neutron scattering and diffraction experiments found no signature of supersolidity [56–59]. Despite the dedicated effort of many groups, there is to date no firm evidence of a supersolid state in solid ^{4}He.

5 Mass Flow through Superfluid-Solid ^{4}He-Superfluid Sandwich

While direct pressure on solid ^{4}He samples failed in inducing mass flow [43–45], Hallock and his collaborators at the University of Massachusetts found evidence of mass flow through solid ^{4}He when a 2 cm thick sample is sandwiched between two superfluid leads, specifically, porous glass Vycor rods filled with superfluid [60–65]. Owing to the small pores in Vycor, the freezing pressure of ^{4}He inside the interconnected pores is elevated to 35 bar, 10 bar above the melting curve, thus allowing a configuration of a solid ^{4}He sample in coexistence with superfluid leads at the same pressure. This superfluid-solid-superfluid or SF-S-SF experimental configuration is also known as the UMass sandwich. The low thermal conductivity of Vycor glass allows the solid ^{4}He sample to be cooled down to below 0.1 K with the high-temperature ends of the Vycor kept near 1.5 K. Conveniently, the thermal conductivity of superfluid infused Vycor is found to be a factor of 3 lower than that of empty Vycor at temperature below 0.5 K [66]. The high-temperature ends of the Vycor rod are opened to small superfluid reservoirs that are connected to room temperature gas handling system via capillaries. Mass flow through solid ^{4}He was found in some but not all samples below 28 bar and 0.6 K. Mass flow rate is determined by recording the pressure versus time at the opposite ends of the SF-S-SF sandwich. In addition to direct gas injection, fountain effect-driven mass flow can also be initiated by imposing heat at one of the bulk superfluid reservoirs. The flow rate of samples with different ^{3}He impurities is shown in Fig. 3. For solid samples prepared

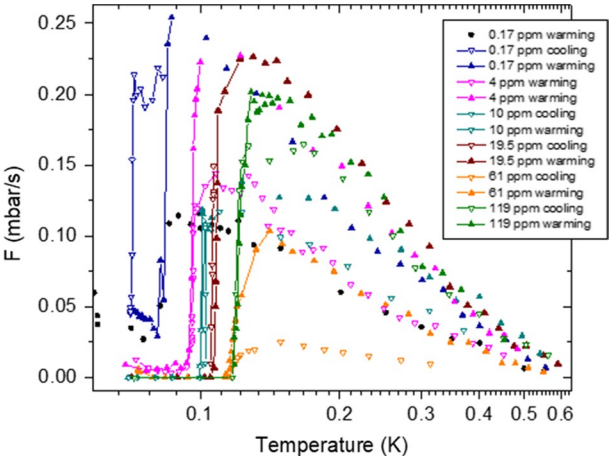

Fig. 3 The temperature dependence of the maximum mass flow rate for different UMass 2 cm thick samples with different ^{3}He impurities and sample histories. Lines are drawn to guide the eye. Figure adapted from [63]. (Color Figure online)

with helium gas with ^{3}He concentration X_3 exceeding 4×10^{-6} the flow rate increases with decreasing temperature and ends abruptly from the maximum value at a temperature T_d near 0.1 K [63–65]. T_d was found to shift to higher temperatures with higher X_3. Quantum Monte Carlo simulation studies proposed that the mass flow is the consequence of transport of ^{4}He atoms along dislocation line with superfluid core [67, 68]. The simulations found both the screw and edge dislocations with a Burgers vector along the c-axis of hcp solid ^{4}He have superfluid core that supports the transport of ^{4}He atoms [67, 68]. In addition, a superclimb process that adds or eliminates basal planes at edge dislocations with a superfluid core was proposed for creating the density gradient in the solid sample in response to the chemical potential that drives the flow through the SF-S-SF sample [68, 69]. In the mass injection measurements, the pressure difference on the opposite sides of the sample cell post-injection appears to approach to zero linearly. This suggests a constant mass flow rate that is independent of the pressure difference across the sample. In the fountain pressure-driven flow, Hallock and collaborators found that the flow rate, F increases sub-linearly with the driving chemical potential difference across the SF-S-SF sandwich in the form of $F=A\ (\Delta\mu)^b$. They found b = 0.35 over the temperature range of the measurement between 0.15 and 0.5 K [64]. This Luttinger liquid-like behavior suggests the mass flow takes place through quasi-one-dimensional channels. While the experiments from UMass found results that are qualitatively in agreement with the quantum Monte Carlo simulation model, a direct *causal* connection between the phenomenon and the dislocation network has not been established. A recent experiment at the University of Alberta reported that it is possible to induce mass flow in a solid ^{4}He sample by direct compression without any superfluid leads [70] and the flow was interpreted to take place along the sample cell wall rather than through solid ^{4}He.

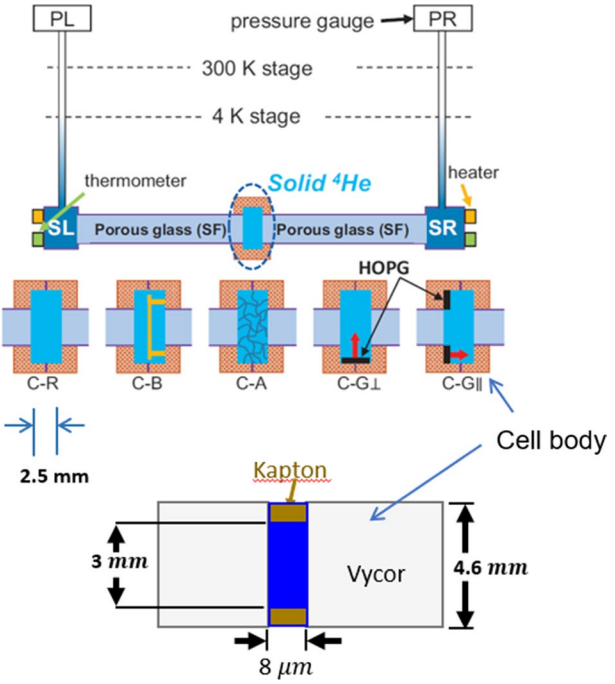

Fig. 4 Schematic drawing showing the experimental configuration and the six different SF-S-SF sample cells used at Penn State. The arrows inside C-G⊥, C-G‖ sample cells show the direction of the c-axes of the HOPG crystalline flakes. Other details of these cells are given in the text. Figure adapted from [72]. (Color figure online)

Chan and his group at Penn State carried out a series of experiments [71–73] to address some of the open questions of this fascinating phenomenon. The questions include: (1) Do the ^{4}He atoms flow directly through the solid, or they are transported along a surface superfluid layer along the cell wall? (2) Is there a causal relation between mass flow and the dislocation network? (3) Is there a specific region on the pressure–temperature phase space where the mass flow phenomenon is allowed? (4) Is the mass flow rate sensitive to the crystal orientation of the solid ^{4}He sample as implied by the superclimb model? (5) How does the flow rate depend on sample pressure and sample thickness? (6) What is the mechanism for the abrupt extinction of mass flow below 0.1 K observed at UMass? (7) Can one gain further insight on the Luttinger liquid behavior?

Chan and his group carried measurements in six different sample cells. The sample cells have the same UMass sandwich geometry and hold solid samples in the shape of cylindrical disks with flow paths along the cylindrical axis. The dimensions of the solid samples in one of the cells are 8 μm thick and 3 mm in diameter. In the other five cells, the samples are ~ 2 mm thick and ~ 10 mm in diameter. These 5 sample cells are designated as C-R, C-B, C-A, C-G⊥ and C-G‖ (See Fig. 4). All sample cells other than C-G‖ use porous Vycor glass rods (4.6 mm diameter and 40 mm in

length) as superfluid leads. Porous glass rods AGC40 (3.5 mm diameter and 40 mm in length), with microstructure similar to that of Vycor, are used in C-G∥. Internal pores in AGC40 have diameter of ~ 4 nm instead of 7 nm. The results from C-R are used as references for the other cells. C-B and C-A have sample dimensions nearly identical to that of C-R (2.5 mm thick and 13.3 mm diameter). C-B has a barrier in the form of a thin Cu foil suspended perpendicular to the flow direction at the center of the sample space. The diameter and cross-sectional area of the Cu foil barrier are, respectively, 96% and 92% of the solid ^{4}He sample. Sample cell C-A is slightly over-packed with a cylindrical disk of silica aerogel of 95% porosity to eliminate any open bulk space inside the cell. Highly oriented pyrolytic graphite crystals (HOPG) flakes are glued in sample cells C-G⊥ and C-G∥ with their c-axes aligned, respectively, perpendicular and parallel to the mass flow direction in an attempt to seed hcp single crystal solid ^{4}He samples with the same alignments.

Prior to the growth of a solid ^{4}He sample, the SF-S-SF cell is filled with superfluid. The solid sample is then grown from superfluid by continually feeding ^{4}He from one capillary to the other to maintain mass flow through the SF-S-SF sandwich while the solid is kept at or below 0.5 K. The high-temperature ends of the Vycor rods are kept below1.5 K so that the rods stay superfluid during the growth process. Mass flow rates are deduced from the pressure versus time readings of the piezo gauges, PR and PL, installed at the room temperature gas manifolds. The mass flow rates, normalized by the cross-sectional areas of the porous glass cylinders are recorded in units of nanogram per second per mm^2 or ng/s/mm^2. As in Hallock's experiments, mass flow can be initiated by injection of ^{4}He into one of the capillaries or by means of superfluid fountain pressure. A fountain pressure can be initiated by adding heat to one of the superfluid reservoirs, SR or SL at the high-temperature ends of the porous glass rods. The measured flow rate is found to be sample dependent, i.e., it is unpredictably different for each new solid sample grown from superfluid.

5.1 Mass Flow Takes Place through Dislocation Network in Solid ^{4}He

The measured flow rate at 0.1 K of the 10 solid ^{4}He samples in C-R varies randomly between 5 and 25 ng/s/mm^2. In comparison, out of the 11 samples measured in C-B with the Cu foil barrier, 8 show no measurable flow and the other three show flow rates of 2.52, 0.69 and 0.49 ng/s/mm^2, a ten-fold reduction compared that in C-R [72]. This means mass flow does take place directly through the body of solid sample and not along a surface superfluid film along the inner walls of the sample cell. Recent measurements from Hallock's group come to the same conclusion [65].

The silica strands of the aerogel in sample cell C-A are randomly interconnected with a mean separation of 100 nm. This is orders shorter than the typical loop length of a dislocation network that exceeds 10 μm. This means a dislocation network cannot form in solid ^{4}He samples grown inside C-A. We grew six solid ^{4}He samples in sample cell C-A and no mass flow is found in any of them below 0.8 K. Above 0.8 K, thermal diffusion induced mass flow is found

[72]. The complete absence of mass flow at low temperature in sample cell C-A together with the results from C-B establishes the *causal* relation that the dislocation network in solid ^{4}He is responsible for the observed mass flow.

Mass flow rate as a function of temperature was measured on 23 solid samples grown in the 8 μm and C-R sample cells with the procedures described above. The pressure of the solid samples studied ranges from the melting curve up to 30 bar. The mass flow rate for all samples decreases with increasing temperature. T_{onset} is the temperature above which mass flow vanishes for a sample at a specific pressure. It is determined by extrapolating the measured flow rate vs. temperature. Figure 5 shows the curve of T_{onset} vs sample pressure. This curve separates the regions with and without mass flow on the pressure–temperature plane. T_{onset} decreases monotonically with increasing sample pressure. It is at 1 K for solid sample at the melting pressure and 0.25 K for solid sample at 30 bar. The reason the T_{onset} values of the 2.5 mm samples show more scatter is because the mass flow rate of the 2.5 mm samples is much lower than that of the 8 μm samples.

If the seeding of crystalline solid ^{4}He by HOPG is successful, the basal plane of the ^{4}He crystals in the C-G∥ cell will be perpendicular to the flow path. With such an orientation, the superclimbing of the edge dislocations, proposed to be crucial for mass flow, will be strongly suppressed [69]. On the other hand, the solid ^{4}He crystal orientation in the C-$G_\perp$ sample cell, if the seeding with HOPG is again successful, will be ideal for the superclimb process. Measurements on the seven and eight solid samples from C-$G_\perp$ and C-G∥ sample cells, however, show similar sample-dependent flow rates that are no different from the C-R cell. The mass flow rates in these three sample cells all vary randomly between 5 to 25 ng/s/mm^2. However, these results do not necessarily invalidate the superclimb model. It is more likely that the attempt to grow crystalline solid ^{4}He samples with the desired orientations in C-G⊥ and C-G∥ is not successful. It is known that there is a strongly bound adsorbed solid ^{4}He layer on the surface of the SiO_2 strands of porous Vycor. This adsorbed layer is

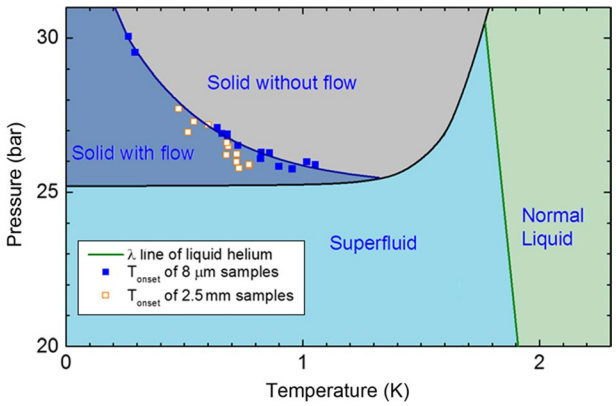

Fig. 5 Boundary separating regions on the P–T plane with and without the mass flow in solid ^{4}He. It corresponds to the plot of $T_{onset,}$ vs pressure. $T_{onset,}$ of a sample at a specific pressure is determined by extrapolating mass flow rate vs. temperature of the sample. Adapted from [71] and supplementary material of [72] (Color figure online)

amorphous with highly disordered atomic structure. Since the growth of solid samples from superfluid starts from this amorphous adsorbed layer, the atomic structure of these starting layers will also be highly disordered and full of defects. The precise structure of these and subsequent layers will be very sensitive to the exact experimental condition that initiated the growth of the solid sample. The structure of these layers in turn plays a dominant role in determining the density and structure of the dislocation network of the solid sample and how the dislocations are 'connected' to the superfluid in the Vycor cylinder. These considerations explain why the mass flow rate is highly sample dependent. In view of the highly disorder nature of the solid in the SF-S interface region, it is not surprising that the C-$G_{\perp}$ and C-G∥ sample cells are not able to confirm the predictions of the idealized superclimb model.

While the mass flow rates are sample dependent, it is still possible to extract the sample thickness dependence of the mass flow rate. The thickness of the solid samples from Penn State and UMass spans from 8 μm to 2 cm. Two plots of mass flow rate vs. sample thickness were made by Shin and Chan [72]. In the first plot, the highest flow rate at 0.1 K among all the samples with pressure between 25.8 to 26.2 bar was used. In the second the average flow rate of samples in the same pressure range measured at 0.15 K was used. In both plots, the mass flow rate shows a robust logarithmic dependence on sample thickness [72].

Once a solid sample is grown from the superfluid, it is possible to densify this 'seed' solid sample by slowly increasing the ^{4}He gas pressure while maintaining mass flow through the SF-S-SF sample cell while keeping the solid sample at a low temperature, e.g., 0.1 K. After a sample has been densified to a higher pressure, it is also possible to de-densify it by lowering the ^{4}He gas pressure gradually, also while maintaining mass flow through the sample. The mass flow rate of solid samples densified or de-densified with this procedure from the same 'seed' solid sample is found to decay exponentially with sample pressure over the pressure range between 25.5 and 27.25 bar. This dependence is found in 9 samples grown in the 8 μm, C-G∥ and the C-R sample cells. The mass flow rate will change unpredictably when a solid sample is melted, and a new 'seed' solid sample is grown from the superfluid.

5.2 Extinction and Recovery of Mass Flow

As shown in Fig. 3, the mass flow rates of the 2 cm thick samples increase in magnitude with decreasing temperature and shut-off abruptly from the maximum value below a temperature T_d near 0.1 K. T_d is found to increase with ^{3}He impurities, X_3, at the few parts per million level. This shut-off or extinction phenomenon was not seen in 8 μm thick solid samples grown with ^{3}He gas with X_3 between 5 parts per billion and 1.5 percent. In solid samples of 2.5 mm in the C-R sample cell, mass flow extinction near 0.1 K is found, but only for samples grown with ^{3}He gas with X_3 that exceeds 2×10^{-3}. After the extinction, the mass flow measured at 0.1 K shows a gradual but complete recovery with a characteristic time of about 10 h. Shin and Chan [73] were able to build a model that explains the results of the 2.5 mm as well as the 2 cm and 8 μm solid samples.

Shin and Chan observed that the extinction of mass flow at low temperature is the consequence of the trapping of ^{3}He atoms at the intersections or nodes of the dislocation network which blocks the mass transport of ^{4}He through the dislocation line. When n, the fraction of the intersections blocked by trapped ^{3}He atoms reaches the percolation threshold, n_c, the mass flow is shut-off. As noted above, shear modulus measurements showed that the stiffening of solid ^{4}He at low temperature is due to the binding of ^{3}He atoms on the dislocation line with a binding energy E_D/k_B equal to 0.7 K [33]. The binding or trapping of ^{3}He should begin at the intersection points of two or more dislocation lines since it is energetically more favorable than elsewhere along the dislocation. The reason why the mass extinction temperature, T_d is found near 0.1 K, about seven times lower than E_D/k_B is the consequence of the much larger configuration space or states available for ^{3}He atoms in the solid sample away from than at the nodes of the dislocation network. Figure 1, adapted from Ref. [33] showed that for a solid ^{4}He sample with $X_3 = 1 \times 10^{-9}$, the dislocation network, including the nodes, is saturated with ^{3}He atoms. The reason why the extinction of mass flow in the 2.5 mm cell is seen only in solid samples grown with helium gas with X_3 exceeding 2×10^{-3}, six orders larger than 1×10^{-9}, is that the great majority of the ^{3}He atoms are filtered into the superfluid in the Vycor rods during the growth of the solid samples. More details on this are provided in the next paragraph on the recovery of mass flow.

The slow recovery of mass flow with a characteristic time of several hours is due to the migration of ^{3}He atoms along the dislocation lines into superfluid in Vycor rods. This migration is 'driven' by the difference in the solubility of ^{3}He in ^{4}He in the liquid and solid phases. At dilute ^{3}He concentrations, ^{3}He atoms are fully miscible in liquid ^{4}He down to 0 K. The solubility of ^{3}He in solid ^{4}He, however, drops exponentially with temperature below 0.5 K. When the solid and liquid phases are in physical contact as in the SF-S-SF sample cells, the binding energy of ^{3}He in favor of superfluid has been calculated to be $E_L/k_B = 1.36$ K [74]. As a result, the equilibrium ratios of ^{3}He concentrations in solid and liquid can be calculated from being close to unity above 0.5 K to $\sim 10^{-4}$ at 0.1 K. There is an additional and larger 'reservoir' for ^{3}He atoms. Measurements on solid ^{4}He-superfluid coexistence systems below 1 K show ^{3}He impurities dissolved in superfluid are preferentially accrued near the solid-superfluid interface. The binding energy E_{SL} of such a surface state is found to be ~ 3 K [75, 76]. Owing to the small pore diameter and high porosity ($\sim 30\%$), porous Vycor glass has a very large internal surface area. The internal pore surface area of the two Vycor rods of C-R is estimated to be 400 m^2 [73]. This means the superfluid-amorphous adsorbed solid layer interface inside the Vycor porous structure is a very large reservoir for ^{3}He atoms.

The sequence of events in the mass flow extinction and recovery phenomenon in the 2.5 mm thick solid sample is as follow: When X_3 of the helium gas mixture exceeds a certain value, which appears to be $\sim 1 \times 10^{-3}$, the superfluid filled Vycor rods are not able to filter out all the ^{3}He impurities within the time scale (~ 10 min) when the solid sample is grown. Once the concentration of ^{3}He in the solid sample exceeds the critical value which is close to 1×10^{-9}, the mass flow is shut-off by ^{3}He atoms trapped at the nodes of the dislocation network. The trapping of the ^{3}He at the nodes of the dislocation is a fast process that occurs within the time scale

in measuring the flow rate, i.e., shorter than a couple of minutes. This is the case because the density of dislocations in solid ^{4}He is on the order of 5×10^8 cm^{-2} and the ^{3}He atoms are always no more than ten μm from a node of the dislocation network. As noted above, the binding energies of ^{3}He in superfluid and particularly at the superfluid-solid interface inside the Vycor pores are larger than that at the nodes of the dislocation nodes. This means that if the low-temperature ends of the Vycor are kept near 0.1 K, ^{3}He atoms are continually migrating along the dislocation lines from the nodes toward the superfluid-infused Vycor rods. The complete mass flow recovery requires all the ^{3}He atoms to migrate through the entire thickness (2.5 mm) of the solid sample. A recent shear modulus experiment studied the migration of ^{3}He atoms along the dislocation line in single-crystal ^{4}He. After stressing the crystal, ^{3}He atoms re-distribute along the dislocation lines. A time scale of 7 h is found for the ^{3}He atoms to return to the equilibrium configuration in the dislocation network at 60 mK[77]. This time scale is in good agreement with the findings of ~ 10 h for full mass flow recovery in the 2.5 mm solid samples at 0.1 K.

The reason why the mass flow shut-off phenomenon is found in the UMass 2 cm thick solid samples grown with much lower ^{3}He impurities than those found in the 2.5 mm cell is that in growing 2 cm solid samples, the great majority of the mixture gas is introduced directly into the sample cell via a third capillary without passing through the two Vycor rods that filter out the ^{3}He impurities [64, 65]. Since the characteristic time of the mass flow recovery phenomenon scales with the dimension of the sample, it is likely that the UMass group did not wait long enough to detect the mass flow recovery phenomenon. The reason why the mass flow shut-off phenomenon is not seen in the 8 μm cell is that the dislocation lines in such thin solid samples are most likely pinned to the Vycor opposing pieces with few or no intersections.

5.3 Luttinger Liquid Flow Properties

The mass flow phenomenon exhibits an interesting and unusual approach toward equilibrium post mass injection and after the heat imposed on one of the superfluid reservoirs is removed. Figure 6 shows the results of a systematic and detailed study of this behavior on an 8 μm solid sample [71]. The left panel shows graphically that PL and PR approach each other linearly until PL = PR after the heat imposed on the superfluid reservoir on the left is removed. Since (PL-PR) corresponds to the chemical potential across the sample and the slope, d(PL-PR)/dt, is proportional to the velocity of mass flow, this means the velocity of mass flow through the solid is independent of the chemical potential driving the flow. This is different from a normal fluid flow through a channel. It is also not consistent with a superfluid, since in a superfluid, there cannot be a pressure gradient across the sample. This behavior is shown in more detail at four different sample temperatures on the right panel. In these plots, the change in the pressure, ΔPR(t) is normalized by the total change, ΔPR(τ), when the pressure PR reaches the equilibrium, i.e., when PR = PL. The time it takes to reach equilibrium, τ, increases with temperature, reflecting the dependence of flow rate on temperature. These plots show [ΔPR(t)/ΔPR(τ)] increases linearly toward the equilibrium immediately after the heat is removed from

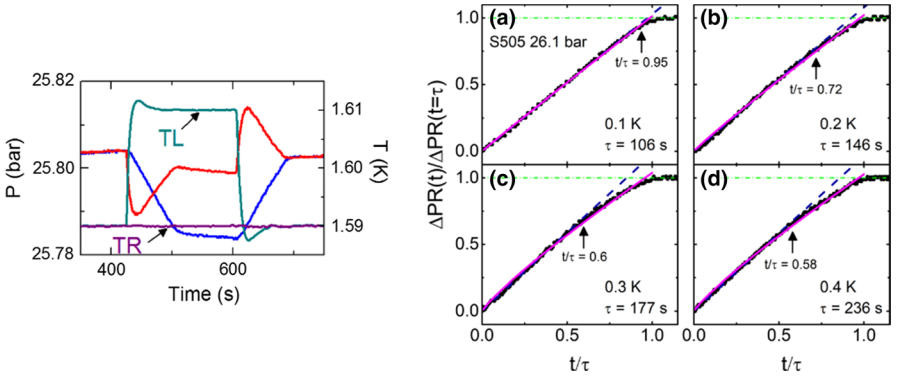

Fig. 6 (Left) Time evolution of PL and PR, pressure readings on the left and right side of a SF-S-SF sample upon the introduction and the removal of a heat pulse to the superfluid reservoir on the left. The heat pulse is marked by the temperature of the reservoir, TL. (Right) Response of the normalized change in PR, $[\Delta PR(t)/\Delta PR(\tau)]$ of sample S505 at 0.1, 0.2, 0.3 and 0.4 K as a function of time, t, starting when the heat pulse on the superfluid reservoir on the left is removed. Equilibrium is reached at $t=\tau$ when PR = PL. The dash blue lines highlight the initial linear dependence of $[\Delta PR(t)/\Delta PR(\tau)]$ on t. The solid purple lines show the fit of Eq. (1). The values of the fitting parameter m are 0.990, 0.960, 0.904 and 0.899 at 0.1, 0.2, 0.3 and 0.4 K, respectively. The values of n are -0.0227, -0.0653, -0.154 and -0.150 at 0.1, 0.2, 0.3 and 0.4 K, respectively. Adapted from [71] (Color figure online)

the reservoir. However, as t approaches τ, a 'tail' appears. At 0.1 K, the deviation from linearity becomes visible for $t/\tau > 0.95$. The deviation appears earlier at smaller value of t/τ and becomes progressively more prominent with higher sample temperatures. We note that similar pressure relaxation behavior, namely nearly linear approach to equilibrium with a tail that becomes more prominent at higher temperature, is seen in another sample [71]. The 'tail' at long t/τ means that the flow velocity decreases with decreasing pressure gradient across the sample. This is expected for a dissipative flow. Interestingly, the data sets can be fitted well between $t/\tau = 0$ and 0.96 with the following functional form with two parameters, m and n;

$$[\Delta PR(t)/\Delta PR(\tau)] \;=\; [m\,(1-n)\,(t/\tau)]^{1/(1-n)} \tag{1}$$

The significance of Eq. (1) and how it is related to the Luttinger liquid behavior of mass flow, to be discussed below, is not clear at this moment.

As noted above, the UMass group reported Luttinger liquid-like mass flow properties. Specifically, the flow rate F driven by fountain pressure is found to increases sub-linearly with the chemical potential difference across the SF-S-SF sandwich, in the form of $F = A(\Delta\mu)^b$. They found $b = 0.35$ over the temperature range of the measurement between 0.15 and 0.5 K [64]. Luttinger liquid behavior in mass flow is also found in the Penn State experiments [71, 72]. The most extensive measurements were carried out on a solid sample of 25.75 bar in sample cell C-GII [72]. Fountain effect driven mass flow rate, F, was measured as a function of δT, the temperature difference of the two superfluid reservoirs. Fifteen sets of measurements, each with the solid sample kept at a different temperature T that

ranges from 45 to 750 mK, were made. Figure 7 shows that the functional form $F = a(\delta T)^b$ provides a good description for the flow rate at different sample temperatures. The value of b appears to be constant at 0.24 for T between 45 and 150 mK but increases rapidly with T for T > 150 mK, reaching 0.5 for T = 750 mK. Similar behaviors are found for two other samples in C-G||, three samples in C-R and one in 8 μm cell. This increase in b above 150 mK probably reflects the onset of thermal dissipation in the mass flow phenomenon.

6 Conclusion

While it is disappointing that the flurry of activities that began in 2004 failed to find credible evidence of supersolidity, the effort did spawn experiments that reveal fascinating physics on solid ^{4}He. The discovery of the giant plasticity effect in solid ^{4}He [78] is an example. Shear modulus measurements by Haziot et.al. on a single ^{4}He crystal free of ^{3}He impurities at 0.1 K found the resistance of the crystal to shear nearly vanishes in one direction. In contrast to other solids, this giant plasticity in solid ^{4}He is completely reversible and manifest itself with an 80% reduction of the elastic constant C_{44}. The mass flow through solid ^{4}He phenomenon discovered by Hallock and collaborators is another example. The experimental results reviewed here show that the transport of ^{4}He atoms through dislocation network is a quintessential physical realization of a Bosonic Luttinger liquid.

Acknowledgments It is an honor for the author to be a student of John Reppy. While he has not always been successful, the author strives to emulate John on how to choose and how best to execute experiments. It is also the great fortune of the author to be a member of the Lee-Reppy-Richardson low-temperature physics group. The friendship and support from them and other members of the LRR group have been invaluable in sustaining the author's scientific career. The author wishes

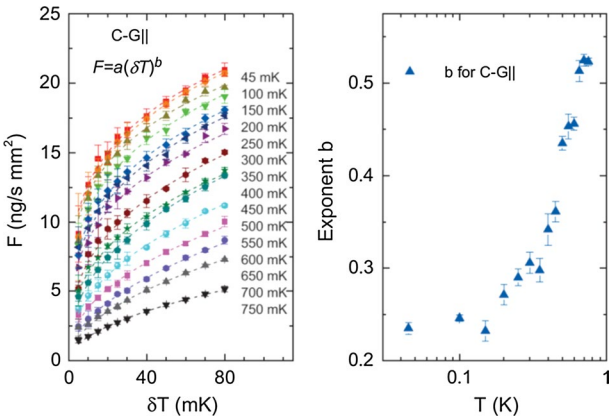

Fig. 7 (Left) Mass flow rate of a solid sample of 25.75 bar in the C-G|| cell at different temperatures as a function of δT, the temperature difference of the superfluid reservoirs. δT is proportional to the fountain pressure. The dashed lines show the fit $F = a(\delta T)^b$. (Right) Value of the exponent b as a function of the solid ^{4}He sample temperature. Adapted from [72] (Color figure online)

to thank the many colleagues, too many to name individually, who are fellow travelers on this solid ^{4}He journey for their friendship and their wisdom. In particular, the author has benefitted enormously in the many conversations with John Reppy, John Beamish, Bob Hallock, Anatoly Kuklov, Phil Anderson, Norbert Mulders, Haruo Kojima and Luciano Reatto. Last but not least, the author wishes to thank his students and post-docs, particularly those who worked with the author on solid ^{4}He: Eunseong Kim, Tony Clark, Xi Lin, Josh West, Zhigang Cheng, Tyler Engstrom, Dukyoung Kim, Ariel Haziot and Jaeho Shin. They have enriched the author's life, in and outside the laboratory. The author is grateful for the help provided by Jaeho Shin and Cui-zu Chang in writing this article. The author also wishes to thank the reviewers of an earlier version of this article for their many insightful suggestions. The functional form of Eq. (1) was suggested by one of the reviewers. The author's work discussed in this review was supported by NSF (DMR) grants 0207071, 0706339, 1103159 and 1707340.

References

1. J.D. Reppy, D. Depatie, Phys. Rev. Lett. **12**, 187 (1964)
2. D.J. Bishop, J.D. Reppy, Phys. Rev. Lett. **40**, 1727 (1978)
3. M.H.W. Chan, K.I. Blum, S.Q. Murthy, G.K.S. Wong, J.D. Reppy, Phys. Rev. Lett. **61**, 1950 (1988)
4. A.F. Andreev, I.M. Lifshitz, Sov. Phys. JETP **29**, 1107 (1969)
5. G.V. Chester, in Lecture in Theoretical Physics, ed. by K.T. Mahanthappa, W.E. Britten. (Gordon& Breach, New York, 1969).
6. G.V. Chester, Phys. Rev. A **2**, 256 (1970)
7. L. Reatto, Phys. Rev. **183**, 334 (1969)
8. A.J. Leggett, Phys. Rev. Lett. **25**, 1543 (1970)
9. H. Suzuki, J. Phys. Soc. Jpn. **35**, 1472 (1973)
10. V.L. Tsymbalenko, JETP Lett. **23**, 653 (1976)
11. D.S. Greywall, Phys. Rev. B **16**, 1291 (1977)
12. G. Bonfait, H. Godfrin, B. Castaing, J. Phys. **50**, 1997 (1989)
13. D.J. Bishop, M.A. Paalanen, J.D. Reppy, Phys. Rev. B **24**, 2844 (1981)
14. P.C. Ho, I.P. Bindloss, J.M. Goodkind, J. Low Temp. Phys. **109**, 409 (1997)
15. J.M. Goodkind, Phys. Rev. Lett. **89**, 095301 (2002)
16. J. Yoon, M.H.W. Chan, Phys. Rev. Lett. **78**, 4801 (1997)
17. M.A. Paalanen, D.J. Bishop, H.W. Dail, Phys. Rev. Lett. **46**, 664 (1981)
18. E. Kim, M.H.W. Chan, Nature **427**, 225 (2004)
19. E. Kim, M.H.W. Chan, J. Low Temp. Phys. **138**, 859 (2005)
20. E. Kim, M.H.W. Chan, Science **305**, 1941 (2004)
21. E.S. Reich, Nature **468**, 748 (2010)
22. A.S.C. Rittner, J.D. Reppy, Phys. Rev. Lett. **97**, 165301 (2006)
23. M. Kondo, S. Takada, Y. Shibayama, K. Shirahama, J. Low Temp. Phys. **148**, 695 (2007)
24. Y. Aoki, J.C. Graves, H. Kojima, Phys. Rev. Lett. **99**, 015301 (2007)
25. B. Hunt, E. Pratt, V. Gadagkar, M. Yamashita, A.V. Balatsky, J.C. Davis, Science **324**, 632 (2009)
26. D.Y. Kim, S. Kwon, H. Choi, H.C. Kim, E. Kim, New J. Phys. **12**, 033004 (2010)
27. R. Toda, P. Gumann, K. Kosaka, M. Kanemoto, W. Onoe, Y. Sasaki, Phys. Rev. B **81**, 214515 (2010)
28. D.E. Zmeev, A.I. Golov, Phys. Rev. Lett. **107**, 065302 (2011)
29. A.D. Fefferman, X. Rojas, A. Haziot, S. Balibar, J.T. West, M.H.W. Chan, Phys. Rev. B **85**, 094103 (2012)
30. N. Mulders, J.T. West, M.H.W. Chan, C.N. Kodituwakku, C.A. Burns, L.B. Lurio, Phys. Rev. Lett. **101**, 165303 (2008)
31. E. Kim, J.S. Xia, J.T. West, X. Lin, A.C. Clark, M.H.W. Chan, Phys. Rev. Lett. **100**, 065301 (2008)

32. M.H.W. Chan, R.B. Hallock, L. Reatto, J. Low Temp. Phys. **172**, 317 (2013)
33. J. Day, J. Beamish, Nature **450**, 853 (2007)
34. J.R. Beamish, A.D. Fefferman, A. Haziot, X. Rojas, S. Balibar, Phys. Rev. B **85**, 180501 (2012)
35. H.J. Maris, Phys. Rev. B **86**, 020502 (2012)
36. X. Rojas, A. Haziot, V. Bapst, S. Balibar, H.J. Maris, Phys. Rev. Lett. **105**, 145302 (2010)
37. A.C. Clark, J.D. Maynard, M.H.W. Chan, Phys. Rev. B **77**, 184513 (2008)
38. D.Y. Kim, J.T. West, T.A. Engstrom, N. Mulders, M.H.W. Chan, Phys. Rev. B **85**, 024533 (2012)
39. J.D. Reppy, Phys. Rev. Lett. **104**, 255301 (2010)
40. D.Y. Kim, M.H.W. Chan, Phys. Rev. B **90**, 064503 (2014)
41. D.Y. Kim, M.H.W. Chan, Phys. Rev. Lett. **109**, 155301 (2012)
42. X. Mi, J.D. Reppy, Phys. Rev. Lett. **108**, 225305 (2012)
43. J. Day, T. Herman, J. Beamish, Phys. Rev. Lett. **95**, 035301 (2005)
44. J. Day, J. Beamish, Phys. Rev. Lett. **96**, 105304 (2006)
45. A.S.C. Rittner, W. Choi, E.J. Mueller, J.D. Reppy, Phys. Rev. B **80**, 224516 (2009)
46. I.A. Todoshchenko, H. Alles, J. Bueno, H.J. Junes, A.Y. Parshin, V. Tsepelin, Phys. Rev. Lett. **97**, 165302 (2006)
47. I.A. Todoshchenko, H. Alles, H.J. Junes, M.S. Manninen, A.Y. Parshin, V. Tsepelin, J. Low Temp. Phys. **150**, 258 (2008)
48. X. Lin, A.C. Clark, M.H.W. Chan, Nature **449**, 1025 (2007)
49. X. Lin, A.C. Clark, Z.G. Cheng, M.H.W. Chan, Phys. Rev. Lett. **102**, 125302 (2009)
50. X. Lin, A.C. Clark, Z.G. Cheng, M.H.W. Chan, Phys. Rev. Lett. **103**, 259903 (2009)
51. L. Yin, J.S. Xia, C. Huan, N.S. Sullivan, M.H.W. Chan, J. Low Temp. Phys. **162**, 407 (2011)
52. L. Yin, J.S. Xia, C. Huan, N.S. Sullivan, M.H.W. Chan, J. Low Temp. Phys. **168**, 257 (2012)
53. Y. Aoki, X. Lin, H. Kojima, Low Temp. Phys. **34**, 329 (2008)
54. S. Kwon, N. Mulders, E. Kim, J. Low Temp. Phys. **158**, 590 (2010)
55. H. Lauter, V. Apaja, I. Kalinin, E. Kats, M. Koza, E. Krotscheck, V.V. Lauter, A.V. Puchkov, Phys. Rev. Lett. **107**, 265301 (2011)
56. S.O. Diallo, R.T. Azuah, O. Kiricheck, J.W. Taylor, H.R. Glyde, Phys. Rev. B **80**, 060504 (2009)
57. H.R. Glyde, J. Low Temp. Phys. **172**, 364 (2013)
58. E. Blackburn, J.M. Goodkind, S.K. Sinha, J. Hudis, C. Broholm, J. van Duijn, C.D. Frost, O. Kirichek, R.B.E. Down, Phys. Rev. B **76**, 024523 (2007)
59. E. Blackburn, J. Goodkind, S.K. Sinha, C. Broholm, L. Copley, R. Erwin, Pramana **71**, 673 (2008)
60. M.W. Ray, R.B. Hallock, Phys. Rev. Lett. **100**, 235301 (2008)
61. M.W. Ray, R.B. Hallock, Phys. Rev. Lett. **105**, 145301 (2010)
62. Y. Vekhov, R.B. Hallock, Phys. Rev. Lett. **109**, 045303 (2012)
63. Y. Vekhov, W.J. Mullin, R.B. Hallock, Phys. Rev. Lett. **113**, 035302 (2014)
64. R.B. Hallock, M.W. Ray, Y. Vekhov, J. Low Temp. Phys. **169**, 264 (2012)
65. R.B. Hallock, J. Low Temp. Phys. **197**, 167 (2019)
66. Z.G. Cheng, M.H.W. Chan, New J. Phys. **15**, 063030 (2013)
67. M. Boninsegni, A.B. Kuklov, L. Pollet, N.V. Prokof'ev, B.V. Svistunov, M. Troyer, Phys. Rev. Lett. **97**, 080401 (2006)
68. S.G. Soyler, A.B. Kuklov, L. Pollet, N.V. Prokof'ev, B.V. Svistunov, Phys. Rev. Lett. **103**, 175301 (2009)
69. A.B. Kuklov, Phys. Rev. B **92**, 134504 (2015)
70. Z.G. Cheng, J. Beamish, Phys. Rev. Lett. **117**, 025301 (2016)
71. J. Shin, D.Y. Kim, A. Haziot, M.H.W. Chan, Phys. Rev. Lett. **118**, 235301 (2017)
72. J. Shin, M.H.W. Chan, Phys. Rev. B **99**, 140502(R) (2019)
73. J. Shin, M.H.W. Chan, Phys. Rev. B **101**, 014507 (2020)
74. D.O. Edwards, S. Balibar, Phys. Rev. B **39**, 4083 (1989)
75. C.L. Wang, G. Agnolet, J. Low Temp. Phys. **89**, 759 (1992)
76. E. Rolley, S. Balibar, C. Guthmann, P. Nozieres, Phys. B (Amsterdam, Neth.) **210**, 397 (1995)
77. X. Rojas, A. Haziot, S. Balibar, J. Phys: Conf. Ser. **400**, 012062 (2012)
78. A. Haziot, X. Rojas, A.D. Fefferman, J.R. Beamish, S. Balibar, Phys. Rev. Lett. **110**, 035301 (2013)